Accepted Manuscript

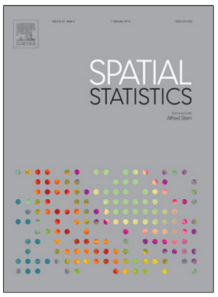

An image quality index based on coefficients of spatial association with an application to image fusion

Silvia M. Ojeda, Grisel M. Britos, Ronny Vallejos

PII: S2211-6753(17)30197-5
DOI: https://doi.org/10.1016/j.spasta.2017.11.003
Reference: SPASTA 271

To appear in: *Spatial Statistics*

Received date : 28 August 2017
Accepted date : 13 November 2017

Please cite this article as: Ojeda S.M., Britos G.M., Vallejos R., An image quality index based on coefficients of spatial association with an application to image fusion. *Spatial Statistics* (2017), https://doi.org/10.1016/j.spasta.2017.11.003

An Image Quality Index Based on Coefficients of Spatial Association with an Application to Image Fusion

Silvia M. Ojeda[a], Grisel M. Britos[a], Ronny Vallejos[b]

[a] *Facultad de Matemática, Astronomía, Física y Computación, Universidad Nacional de Córdoba Medina Allende S/N, Córdoba, Argentina*

[b] *Departamento de Matemática, Universidad Técnica Federico Santa María Casilla 110-V, Valparaíso, Chile*

Abstract

In the last decade, image quality indices have received considerable attention to quantify the dissimilarity between two images. The codispersion coefficient, commonly used in spatial statistics to address the association between two processes has also been used for this aim. Here we introduce an image quality index (CQ_{max}) that is based on codispersion. This new coefficient is a directional evaluation of the spatial association, and consists on computing the maximum codispersion for a finite set of spatial lags on the plane, which also allows to obtain the direction associated with the maximum codispersion. From the CQ_{max} index, a pseudo-metric that can be used as a cost functional for related optimization problems is defined. We carry out Monte Carlo simulations to explore the performance of the proposed index and its capability to detect directional contaminations. Additionally, we introduce a novel algorithm to restore directionally contaminated images and present an application with real data in the context of image fusion.

Key words: Image similarity, **SSIM index**, CQ_{max} index, Spatial lag, Image fusion.

1. Introduction and Motivation

The enormous development of the technological resources of the last decades has been a determining factor in the construction and implementation of different coefficients and quality measures to quantify the similarity between two digital images. In spite of the different initiatives that have been developed so far, this line of research is a recent one; and therefore the design, definition, and study of new ideas remain as objectives of notable interest in mathematics, computation and statistical image processing.

Similarity and quality are strongly related notions when comparing digital images. The image quality analysis (IQA) is linked to the assessment of image quality derived from human judgment. In general, IQA can be classified into subjective IQA and objective IQA (Wang and Bovik, 2009). The subjective perspective is widely accepted as the most accurate approach to measuring quality, since the human eye is the ultimate

receiver of the majority, but of all visual communication systems. In recent decades, the most significant contribution of subjective IQA is probably the construction of databases consisting of digital images with various types of distortions and their subjective ratings recorded with the **Mean Opinion Score (MOS) index**. The most widely used databases are the Tampere Image Database 2008 (TID2008) (Ponomarenko et al., 2009), the Tampere Image Database 2013 (TID2013) (Ponomarenko et al., 2013), and the Categorical Subjective Image Quality (CSIQ) database (Larson and Chandler, 2010).

Frequently used objective quality measures in image processing are the Mean Square Error (MSE) and the Peak Signal to Noise Ratio (PSNR). Both measures have shown a poor correlation with the MOS index in practical applications **(Eckert and Bradley, 1998; Wang et al., 2004)**. In order to overcome this inconvenience, Wang and Bovik (2002) suggested the structural similarity index (SSIM). This measure is based on the reasonable assumption that human visual perception is strongly adapted to extract structural information from a scene. The SSIM index relates the luminance, contrast and structural similarity between two images to be compared. Since the introduction of SSIM, a number of extensions of the SSIM have been published and discussed (Wang and Bovik, 2009). Some of them are the multiscale SSIM index (Wang et al., 2003), the visual information fidelity (Sheikh and Bovik, 2006), the visual signal-to-noise ratio (Chandler and Hemami, 2007), the most apparent distortion measure (Larson and Chandler, 2010), the information content-weighted method (Wang and Li, 2011), the feature similarity index (Zhang et al., 2011), the SSIM-motivated rate-distortion optimization for video coding (Wang et al., 2012), Perceptual quality assessment for multi-exposure image fusion, (Ma et al., 2015), among others.

In spatial statistics the association between two random fields (images) has been treated in several different fashions. Extensions of the well known Pearson correlation coefficient have been studied and implemented in order to capture the existing directional autocorrelation of each process. On the other hand, a generalization of the coefficients commonly used in multivariate analysis was implemented to account for the correlation between two variables which take values in general manifolds (Jupp and Mardia, 1980; Crosby et al., 1993). As an extension of the correlation coefficient, Matheron (1965) introduced a measure of spatial association between two spatial variables called the codispersion coefficient. This coefficient has been studied recently under several different perspectives. For example Rukhin and Vallejos (2008) studied the limiting distribution of the sample coefficient. Vallejos (2008) and Vallejos (2012) **addressed the coefficient to measure the comovement between two time series**. Cuevas et al. (2013) developed a Nadaraya-Watson-type estimator for the codispersion. The computational implementation of certain routines currently available in the R package SpatialPack has been addressed in Osorio et al. (2012). In the context of classification of satellite images, Vallejos et al. (2015a) defined a codispersion matrix to assess the association of a spatial vector of dimension m. Buckley et al. (2016a,b) used the codispersion coefficient to describe and visualize complex spatial patterns of multiple co-occurring variables in ecology. The association between two spatial processes can be addressed also from an hypothesis testing perspective (See for instance Clifford et al.,

1989; Dutilleul, 1993, 2008).

In the image quality assessment framework, Ojeda et al. (2012) introduced a variant of the SSIM that is able to capture the hidden spatial correlation between two images. This feature is obtained by considering the codispersion coefficient instead of the sample correlation coefficients as part of the SSIM. This proposal (CQ) depends on a specific spatial lag defined on the two-dimensional space in the same way as the cross-variogram. Later, Vallejos et al. (2016) extended the known mathematical properties established for the SSIM to the CQ index. Suitable distance measures associated with the CQ index were defined, and the quasi-convexity was established for the distances associated with the CQ coefficient.

In this paper, we define an image similarity index, called $\text{CQ}_{\max}$ that has been preliminary explored by Pistonesi et al. (2015), and consists of evaluating the CQ coefficient between the images to be compared, for many directions (lags) on the space. The $\text{CQ}_{\max}$ index is the maximum value of CQ for those values that are greater than a certain threshold. This provides a global coefficient that does not depend on the spatial lag on the space. As a consequence, we define a pseudo-metric that is associated with the new index, and preserves the information contained in $\text{CQ}_{\max}$. We carry out Monte Carlo simulation experiments to explore the performance of the $\text{CQ}_{\max}$ index with respect to other coefficients of the same type. We also conduct a numerical experiment to observe the behavior of the coefficient when there is directional contamination (Cheung et al., 2000). In the context of image fusion, a novel image restoration algorithm that recovers directionally contaminated images is introduced. This algorithm relies on the capability of coefficient $\text{CQ}_{\max}$ to detect the direction of maximum codispersion on the space. Numerical experiments with real images from the TID2008 database provide more insight into the quality of the algorithm for restoring images contaminated with 17 different types of noise. As a result, the suggested index behaves better than existing coefficients based on the codispersion, and is the basis for the construction of the restoration algorithm depicted in Section 5.

The R code and databases used in the numerical experiments are available in a supplementary material for this paper.

2. Preliminaries and Notation

In this paper, we let $\mathbb{R}_+$ denote the nonnegative real line, and $\mathbb{R}_+^N, N \in \mathbb{N}$, denote the first orthant, i.e., the set of N-dimensional vectors with nonnegative components. Let $(\Omega, \mathcal{A}, P)$ be a probability space, define

$$W = \{(i,j) \in \mathbb{Z}^2 : 1 \leq i \leq n, 1 \leq j \leq m\}, \tag{1}$$

where $m, n \in \mathbb{N}$, and let $X : \Omega \to \Lambda$ be a spatial process, where Λ is the set of functions from W to $\mathbb{R}_+$. A realization of X will be characterized by a matrix denoted by $\boldsymbol{X} \in \mathcal{M}^{n\times m}(\mathbb{R})$ where $\boldsymbol{X}(i,j)$ indicates the level of gray intensity at the position (i,j). Alternatively, a realization of X can be charecterized by a vectorization of matrix $\boldsymbol{X}$, given by $\boldsymbol{x} = \text{vec}(\boldsymbol{X}) = (\boldsymbol{x}_1^T, ..., \boldsymbol{x}_N^T)^T$, with

$N = m \cdot n$ **(Brunet et al., 2012; Vallejos et al., 2016). In this work we use both representations for a realization of** X.

If $\boldsymbol{x}, \boldsymbol{y} \in \mathbb{R}_+^N$ are two images, the SSIM index is

$$\text{SSIM}(\boldsymbol{x}, \boldsymbol{y}) = l(\boldsymbol{x}, \boldsymbol{y})^\alpha \cdot c(\boldsymbol{x}, \boldsymbol{y})^\beta \cdot s(\boldsymbol{x}, \boldsymbol{y})^\gamma \tag{2}$$

where α, β and γ are parameters that are associated with the weight of each multiplicative coefficient

$$l(\boldsymbol{x}, \boldsymbol{y}) = \left(\frac{2\bar{x}\bar{y} + c_1}{\bar{x}^2 + \bar{y}^2 + c_1} \right), \tag{3}$$

$$c(\boldsymbol{x}, \boldsymbol{y}) = \left(\frac{2s_{\boldsymbol{x}} s_{\boldsymbol{y}} + c_2}{{s_{\boldsymbol{x}}}^2 + {s_{\boldsymbol{y}}}^2 + c_2} \right), \tag{4}$$

$$s(\boldsymbol{x}, \boldsymbol{y}) = \left(\frac{s_{\boldsymbol{xy}} + c_3}{s_{\boldsymbol{x}} s_{\boldsymbol{y}} + c_3} \right), \tag{5}$$

with $\bar{x}$, $\bar{y}$, $s_{\boldsymbol{x}}^2$, $s_{\boldsymbol{y}}^2$ and $s_{\boldsymbol{xy}}$ that represent the sample means of $\boldsymbol{x}$ and $\boldsymbol{y}$, the sample variances of $\boldsymbol{x}$ and $\boldsymbol{y}$, and the sample covariance between $\boldsymbol{x}$ and $\boldsymbol{y}$, respectively. Here, we consider the balanced case, i.e., $\alpha = \beta = \gamma = 1$. The constants c_1, c_2, and c_3 are all **nonnegative** and can be settled down in such a way that preserve the definition of the SSIM index when the denominators are close to zero. Commonly these constants are small real numbers included to avoid instability when $\bar{x} + \bar{y}$ is close to zero (Wang et al., 2004).

The CQ index arose from the need of an image quality measure that quantifies the similarity between two images in a particular spatial lag $\boldsymbol{h}$, in a similar fashion as the variogram is defined for one spatial process. For $\boldsymbol{h} = (h_1, h_2)$ the CQ coefficient is defined through (Ojeda et al., 2012)

$$\text{CQ}(\boldsymbol{x}, \boldsymbol{y}, \boldsymbol{h}) = l(\boldsymbol{x}, \boldsymbol{y})^\alpha \cdot c(\boldsymbol{x}, \boldsymbol{y})^\beta \cdot s_c(\boldsymbol{x}, \boldsymbol{y}, \boldsymbol{h})^\gamma, \tag{6}$$

where $l(\boldsymbol{x}, \boldsymbol{y})$ and $c(\boldsymbol{x}, \boldsymbol{y})$ are as in Equations (3) and (4), respectively, and $s_c(\boldsymbol{x}, \boldsymbol{y}, \boldsymbol{h})$ is the sample codispersion coefficient defined as (Rukhin and Vallejos, 2008)

$$s_c(\boldsymbol{x}, \boldsymbol{y}, \boldsymbol{h}) = \frac{\langle \boldsymbol{A_h x}, \boldsymbol{A_h y} \rangle + c_3}{||\boldsymbol{A_h x}|| \cdot ||\boldsymbol{A_h y}|| + c_3}, \tag{7}$$

where $c_3 \geq 0$, $\boldsymbol{A_h} : \mathbb{R}^N \longrightarrow \mathbb{R}^{N_h}$ is a linear function where $\boldsymbol{A_h x} := \boldsymbol{x_h} := (x_k - x_{k+h^*})_{k \in S_{\boldsymbol{h}}^{im}}$, $h^* = h_1 + nh_2$, $S_{\boldsymbol{h}}^{im} = \{k : 1 \leq k \leq nm \ \wedge \ F^{-1}(k) \in S_{\boldsymbol{h}}\}$, $F : \mathbb{Z}_+^2 \longrightarrow \mathbb{Z}_+$ is the natural map associated with the index $F(i, j) = j + (n-1)i = k$, $S_{\boldsymbol{h}} = \{s \in S : s + \boldsymbol{h} \in D\}$, $S = \{s_1, ..., s_k\} \subset D \subset \mathbb{R}^2$, $N_{\boldsymbol{h}} = |S_{\boldsymbol{h}}|$, $||\cdot||$ is the Euclidean norm and $< \cdot, \cdot >$ is the inner product of $\mathbb{R}^{N_{\boldsymbol{h}}}$. If $c_3 = 0$, $s_c(\boldsymbol{x}, \boldsymbol{y}, \boldsymbol{h})$ coincides with the empirical version of the codispersion coefficient between $\boldsymbol{x}$ and $\boldsymbol{y}$ (Vallejos et al., 2016).

Contrarily to the SSIM index the CQ coefficient depends on the spatial lag $\boldsymbol{h}$, **a separation vector between observations** $X(\boldsymbol{s})$ **and** $X(\boldsymbol{s}+\boldsymbol{h})$. In practice, there are

at least two ways of choosing suitable values of $\boldsymbol{h}$ depending on the available knowledge about a certain direction of interest. If there is information about $\boldsymbol{h}$, the CQ index can be computed in that particular direction. Otherwise, a grid can be constructed on the plane where the coefficient can be computed for all elements of the grid. A graph where the intensities of the coefficient versus the coordinates of the grid can be constructed similarly to the way the variogram map is built (Isaaks and Srivastava, 1989). This technique, has been studied and discussed by Vallejos et al. (2015b) and Buckley et al. (2016a).

The CQ coefficient has been used to construct distance measures between images. For two images $\boldsymbol{x}$ and $\boldsymbol{y}$ Vallejos et al. (2016) defined

$$d_1(\bar{x}, \bar{y}) = \frac{|\bar{x} - \bar{y}|}{\sqrt{\bar{x}^2 + \bar{y}^2 + c_1}}, \tag{8}$$

$$d_2(s_{\boldsymbol{x}}, s_{\boldsymbol{y}}) = \frac{|s_{\boldsymbol{x}} - s_{\boldsymbol{y}}|}{\sqrt{s_{\boldsymbol{x}}^2 + s_{\boldsymbol{y}}^2 + c_2}}, \tag{9}$$

$$d_3(\boldsymbol{x}, \boldsymbol{y}, \boldsymbol{h}) = \sqrt{1 - \left(\frac{\langle \boldsymbol{A_h x}, \boldsymbol{A_h y} \rangle}{||\boldsymbol{A_h x}||.||\boldsymbol{A_h y}||}\right)^2}, \tag{10}$$

and

$$\boldsymbol{d}_{CQ_{\boldsymbol{h}}}(\boldsymbol{u}, \boldsymbol{v}) = (d_1(\bar{u}, \bar{v}), d_2(s_{\boldsymbol{u}}, s_{\boldsymbol{v}}), d_3(\boldsymbol{u}, \boldsymbol{v}, \boldsymbol{h}))^\top,$$

where c_1 and c_2 are non negative constants, and $\boldsymbol{h}$ is a fixed spatial lag. The same authors proved that the function defined as

$$d_{CQ_{\boldsymbol{h}}}(\boldsymbol{x}, \boldsymbol{y}) = ||\boldsymbol{d}_{CQ_{\boldsymbol{h}}}(\boldsymbol{x}, \boldsymbol{y})||_2 \tag{11}$$

is a pseudo metric in $\mathbb{R}_+^N$.

3. The $\mathrm{CQ}_{\max}$ Coefficient

Here we introduce a new image quality measure, labeled $\mathrm{CQ}_{\max}$, which is based on the CQ coefficient (Ojeda et al., 2012) for a finite set of spatial lags on the space. The maximum value of the CQ coefficient computed using all spatial lags such that the CQ is greater than a certain threshold provides a coefficient that is independent of the direction as is stated in the following definition.

Definition 1. Let $\boldsymbol{x}, \boldsymbol{y} \in \mathbb{R}_+^N$ be two images, W as in (1) and $H_W = \{\boldsymbol{h} \in \mathbb{Z}^2 : \boldsymbol{s} + \boldsymbol{h} \in W, \boldsymbol{s} \in W\}$. The $\mathrm{CQ}_{\max}$, coefficient between images $\boldsymbol{x}$ and $\boldsymbol{y}$ is

$$\mathrm{CQ}_{\max}(\boldsymbol{x}, \boldsymbol{y}) = \max_{\{\boldsymbol{h} \in H_W:\ p(\boldsymbol{h}) \geq p_0\}} |\mathrm{CQ}(\boldsymbol{x}, \boldsymbol{y}, \boldsymbol{h})|, \tag{12}$$

where $p_0 \in (0, 1)$ is a known threshold, and $p\,(\cdot)$ is the proportion of pixels in the image associated with the computation of CQ in the direction $\boldsymbol{h}$.

The $\mathrm{CQ}_{\max}$ coefficient is a directional evaluation of the codispersion in a neighborhood of directions of interest on the plane, and looks for the maximum spatial association **between** the variables over a finite set of directions. **Because there exist at least one direction in H_W that involves all pixels of the image, the computation of the $\mathrm{CQ}_{\max}$ index indeed considers the edges according with Equation (12).**

Following the work of Brunet et al. (2012) we define a distance between two images based on the $\mathrm{CQ}_{\max}$ coefficient. According to Definition 1 there is at least one $\boldsymbol{h}_0 \in H_W$ such that $\mathrm{CQ}_{\max}(\boldsymbol{x}, \boldsymbol{y}) = \mathrm{CQ}(\boldsymbol{x}, \boldsymbol{y}, \boldsymbol{h}_0)$. Then a natural candidate to measure the distance between images $\boldsymbol{x}$ and $\boldsymbol{y}$ is $D_{\mathrm{CQ}_{\max}}(\boldsymbol{x}, \boldsymbol{y}) = d_{\mathrm{CQ}_{\boldsymbol{h}_0}}(\boldsymbol{x}, \boldsymbol{y})$ where $d_{\mathrm{CQ}_{\boldsymbol{h}}}$ is as in (11).

The spatial lag $\boldsymbol{h}_0$ is not unique. Indeed, if

$$\boldsymbol{X} = \begin{pmatrix} 1 & 0 \\ 1 & 1 \end{pmatrix} \qquad \boldsymbol{Y} = \begin{pmatrix} 1 & 1 \\ 0 & 1 \end{pmatrix},$$

the maximum codispersion is 0, which is obtained for $\boldsymbol{h} = (1, 0)$ and $\boldsymbol{h} = (0, 1)$. An alternative distance is given in the following definition.

Definition 2. Let $\boldsymbol{x}, \boldsymbol{y} \in \mathbb{R}_+^N$ be two images. Let d_{CQ_h} as in (11) and let p_0, W, and H_W be as in Definition 1. We define

$$D_{CQ_{\max}}(\boldsymbol{x}, \boldsymbol{y}) = \max_{\{\boldsymbol{h} \in H_W:\ p(\boldsymbol{h}) \geq p_0\}} d_{CQ_{\boldsymbol{h}}}(\boldsymbol{x}, \boldsymbol{y}). \tag{13}$$

Proposition 1. $D_{CQ_{\max}}(\cdot, \cdot)$ is a pseudo-metric in $\mathbb{R}^N$.

Proof. The facts that $D_{\mathrm{CQ}_{\max}}(\boldsymbol{x}, \boldsymbol{y})$ is positive and symmetric are inherited from $d_{\mathrm{CQ}_{\boldsymbol{h}}}$. Now, given $\boldsymbol{h} \in \{\boldsymbol{h} \in H_W : p(\boldsymbol{h}) \geq p_0\}$, $d_{\mathrm{CQ}_{\boldsymbol{h}}}$ satisfies the triangular inequality $d_{\mathrm{CQ}_{\boldsymbol{h}}}(\boldsymbol{x}, \boldsymbol{y}) \leq d_{\mathrm{CQ}_{\boldsymbol{h}}}(\boldsymbol{x}, \boldsymbol{z}) + d_{\mathrm{CQ}_{\boldsymbol{h}}}(\boldsymbol{z}, \boldsymbol{y})$. Thus, applying the maximum in both sides of the last equation we have that

$$\begin{aligned} D_{\mathrm{CQ}_{\max}}(\boldsymbol{x}, \boldsymbol{y}) &= \max_{\{\boldsymbol{h} \in H_W:\ p(\boldsymbol{h}) \geq p_0\}} d_{\mathrm{CQ}_{\boldsymbol{h}}}(\boldsymbol{x}, \boldsymbol{y}) \\ &\leq \max_{\{\boldsymbol{h} \in H_W:\ p(\boldsymbol{h}) \geq p_0\}} (d_{\mathrm{CQ}_{\boldsymbol{h}}}(\boldsymbol{x}, \boldsymbol{z}) + d_{\mathrm{CQ}_{\boldsymbol{h}}}(\boldsymbol{z}, \boldsymbol{y})) \\ &\leq \max_{\{\boldsymbol{h} \in H_W : p(\boldsymbol{h}) \geq p_0\}} d_{\mathrm{CQ}_{\boldsymbol{h}}}(\boldsymbol{x}, \boldsymbol{z}) + \max_{\{\boldsymbol{h} \in H_W:\ p(\boldsymbol{h}) \geq p_0\}} d_{\mathrm{CQ}_{\boldsymbol{h}}}(\boldsymbol{z}, \boldsymbol{y}) \\ &= D_{\mathrm{CQ}_{\max}}(\boldsymbol{x}, \boldsymbol{z}) + D_{\mathrm{CQ}_{\max}}(\boldsymbol{z}, \boldsymbol{y}). \end{aligned}$$

Thus $D_{\mathrm{CQ}_{\max}}$ is a pseudo-metric. □

It should be emphasized that (11) and (13) imply that

$$D_{\mathrm{CQ}_{\max}}(\boldsymbol{x}, \boldsymbol{y}) = \sqrt{d_1(\bar{\boldsymbol{x}}, \bar{\boldsymbol{y}})^2 + d_2(s_{\boldsymbol{x}}, s_{\boldsymbol{y}})^2 + \left(\max_{\{\boldsymbol{h} \in H_W:\ p(\boldsymbol{h}) \geq p_0\}} d_3(\boldsymbol{x}, \boldsymbol{y}, \boldsymbol{h}) \right)^2}. \tag{14}$$

Then, if images $\boldsymbol{x}, \boldsymbol{y} \in \mathcal{F}_{\mu,\sigma} = \{\boldsymbol{x} \in \mathbb{R}_+^N : \bar{x} = \mu,\ s_{\boldsymbol{x}} = \sigma\}$,

$$D_{\mathrm{CQ}_{\max}}(\boldsymbol{x}, \boldsymbol{y}) = \max_{\{\boldsymbol{h} \in H_W:\ p(\boldsymbol{h}) \geq p_0\}} d_3(\boldsymbol{x}, \boldsymbol{y}, \boldsymbol{h})$$
$$= \max_{\{\boldsymbol{h} \in H_W:\ p(\boldsymbol{h}) \geq p_0\}} \sqrt{1 - \left(\frac{\langle \boldsymbol{A_h x}, \boldsymbol{A_h y} \rangle}{||\boldsymbol{A_h x}|| \cdot ||\boldsymbol{A_h y}||} \right)^2}. \quad (15)$$

In this case, for $\boldsymbol{y}$ fixed, it is possible to find a minimum of $D_{\mathrm{CQ}_{\max}}(\boldsymbol{x}, \boldsymbol{y})$ when $\boldsymbol{x}$ is in the convexity region of the function $\frac{\langle \boldsymbol{A_h x}, \boldsymbol{A_h y} \rangle}{||\boldsymbol{A_h x}||.||\boldsymbol{A_h y}||}$, along the lines given by Vallejos et al. (2016).

For practical applications, the pseudo-metric obtained from the modification of the $\mathrm{CQ}_{\max}$ index is essentially equivalent to the original coefficient. This result is shown via a numerical example in which the databases TID2008 and TID2013 have been used. Figure 1 displays an inverse and non-linear association between $\mathrm{CQ}_{\max}$ and $D_{\mathrm{CQ}_{\max}}$. The results, as expected, are slightly better for the TID2008 database which contains less types of contaminations than the TID2013 database.

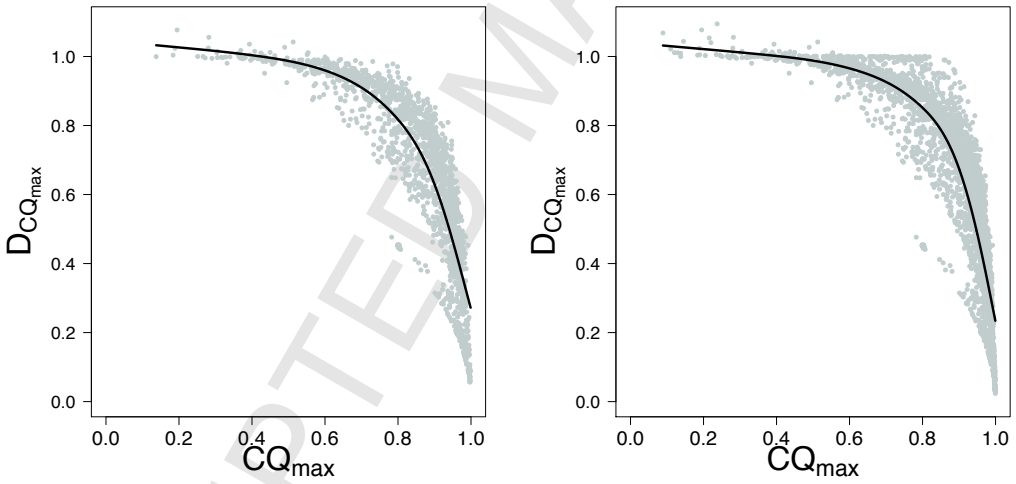

(a) (b)

Figure 1: (a) $\mathrm{CQ}_{\max}$ versus $D_{\mathrm{CQ}_{\max}}$ for the TID2008 database; (b) $\mathrm{CQ}_{\max}$ versus $D_{\mathrm{CQ}_{\max}}$ for the TID2013 database. The solid line in each case corresponds to a spline fit made with the R function `smooth.spline`.

In definition 1 the $\mathrm{CQ}_{\max}$ coefficient was defined for a fixed value of p_0. Because p_0 is the proportion of pixels used in the computation of CQ for a fixed $\boldsymbol{h}$, intuitively p_0 could be chosen as a large value belonging to the interval $(0, 1)$, to ensure the quality of the CQ estimates. Beyond that, by the knowledge acquired from numerical experiments, practical rules can be implemented. As an illustration, we computed the $\mathrm{CQ}_{\max}$ index

between the 25 images belonging to the TID2008 database with the corresponding contaminated images with Gaussian additive noise at level of intensity 2. Using the same database the experiment was repeated for impulsive noise. In Figure 2 we plotted $\mathrm{CQ}_{\max}$ versus p_0, for $p_0 \in \{0.75, 0.8, 0.85, 0.9, 0.95\}$ for both types of noise. A decreasing pattern for the mean value is observed when p_0 increases, a slightly increase in variance is also observed when p_0 increases. As a result, if the goal is to preserve the value of $\mathrm{CQ}_{\max}$ in the interval $(0.85, 0.90)$, p_0 should be chosen within the range $(0.75, 0.80)$. **In practical applications where there is no previous knowledge about p_0, a training set of images could be used to obtain initial estimates. In the numerical experiments described in the next section we consider $p_0 = 0.75$ as a parsimonious estimate, however, the results of the image restoration algorithm that will be introduced in Section 5, will not change significantly if p_0 varies.**

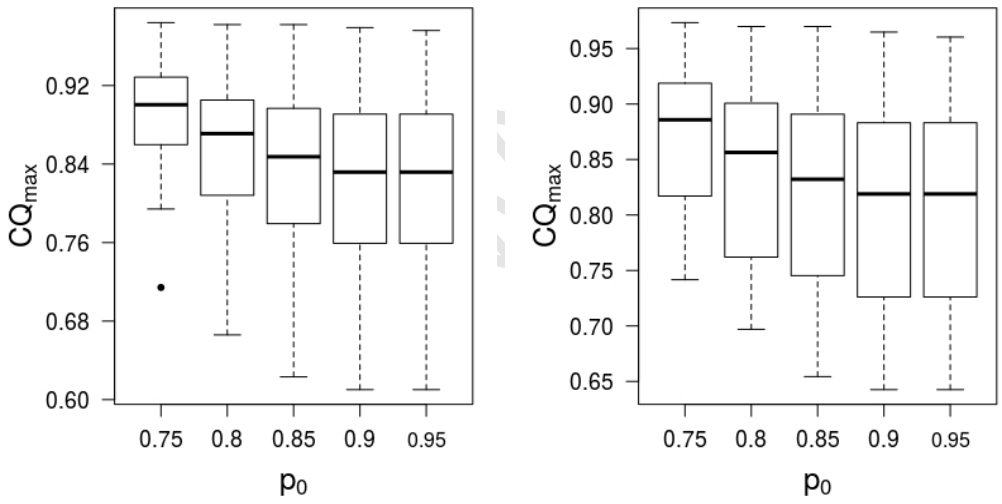

(a) (b)

Figure 2: (a) $\mathrm{CQ}_{\max}$ between the 25 original images of the database TID2008 and the corresponding contaminated images with additive Gaussian noise at level 2; (b) $\mathrm{CQ}_{\max}$ between the 25 original images of the database TID2008 and the corresponding contaminated images with impulsive noise at level 2.

4. Numerical Experiments

In this section we introduce two experiments with real images in order to explore the performance of the $\mathrm{CQ}_{\max}$ coefficient with respect to the mean opinion score (MOS) index (Ponomarenko et al., 2009), and the effect of the directional contamination on a reference image.

4.1. Performance of $CQ_{\max}$

An experiment was designed to inspect how close the $CQ_{\max}$ of the human visual criterion is to compare images. In order to have consistent measures for a large set of images we compare the MOS coefficient with the $CQ_{\max}$ for the 1700 images contained in the TID2008 database. This means that both coefficients were measured for each pair of images belonging to the TID2008 database. In addition, coefficients CQ(1,1), MSE and SSIM were included in the study. The results are displayed in Figure 3.**The correlation coefficient between the MSE and MOS is -0.2895 and between the SSIM and MOS 0.4578 (Figure 3 (c) and (d)). However, there is a clear linear correlation between the CQ(1,1) and MOS (0.6068) and between the $CQ_{\max}$ with the MOS (0.6089) (see Figure 3 (a) and (b)).** This result is surprising because the SSIM index was constructed to improve the behavior of the MSE with respect to the human visual system (Wang et al., 2004), but this experiment is showing that the CQ(1,1) and $CQ_{\max}$ have a better performance than the MSE and SSIM when they are used to represent the human visual system for this particular database. The performance of the CQ(1,1) and $CQ_{\max}$ **coefficients are comparable.**

Table 1: Kendall and Spearman coefficients between the indices SSIM, CQ(1,1), and $CQ_{\max}$, and the MOS, for all images belonging to the TID2008 database.

Index	Kendall	Spearman
SSIM	0.4187	0.5997
	(0.3950, 0.4420)	(0.5681, 0.6288)
CQ(1,1)	0.3964	0.5609
	(0.3690, 0.4240)	(0.5232, 0.5936)
$CQ_{\max}$	**0.4383**	**0.6183**
	(0.4120, 0.4620)	(0.5858, 0.6473)

In order to quantify the discrepancies among these coefficients with respect to the MOS, the Spearman and Kendall correlation coefficients **(Brunet et al., 2012; Ponomarenko et al., 2013)** between the MOS and each one of the image quality coefficients considered in this study were computed for the images belonging to the TID2008 database. The results displayed in Table 1 show that the $CQ_{\max}$ index has the larger association with the MOS exceeding the correlation values associated with the CQ(1,1) and SSIM indices. **In each case, 95% confidence intervals (Hollander et al., 2014, Sec. 8.3 and 8.4) were contructed for each coefficient. From the point estimates there is evidence in favor of $CQ_{\max}$ with respect to the other coefficients; nevertheless, there is no significant differences between the estimates because the confidence intervals overlap**. Thus, there is relative empirical evidence in favor of the $CQ_{\max}$ index for representing the human visual system. In addition, indices $CQ_{\max}$, CQ(1,1) and SSIM were compared when the images

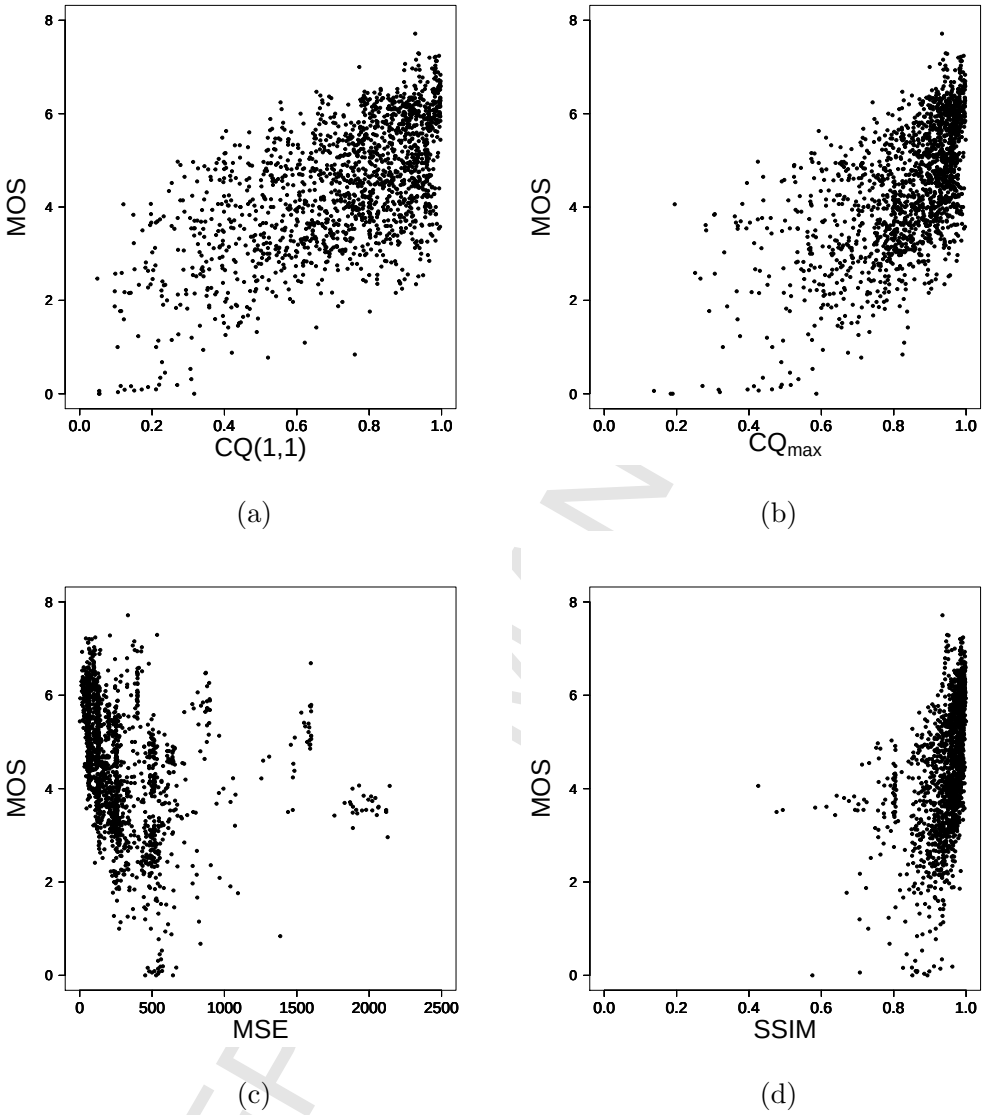

Figure 3: For the TID2008 database: (a) $CQ_{(1,1)}$ versus MOS; (b) CQ_{max} versus MOS; (c) MSE versus MOS; (d) SSIM versus MOS.

belonging to the TI2008 database were classified into three groups. The first group, called Bad quality (BQ), corresponds to those images that have a MOS index with the original one ranging from 0 to 3.9394. The second group, called Middle quality (MQ), corresponds to those images having a MOS index ranging from 3.9394 to 5.1714. The third group, called Good quality (GQ), includes images with MOS larger than 5.1714. Table 2 shows Spearman and Kendall coefficients for the three groups of images. In-

Table 2: Spearman and Kendall rank order correlation coefficients between MOS and the quality measures SSIM, CQ, and CQ_{max} when the TID2008 database has been clasiffied into three groups: BQ, MQ, and GQ.

	Spearman			Kendall		
Index	BQ	MQ	GQ	BQ	MQ	GQ
SSIM	0.3400	0.1325	0.3095	0.2386	0.0887	0.2127
CQ(1,1)	**0.4495**	0.0855	**0.4114**	0.3160	0.0573	**0.2791**
CQ_{max}	0.4481	**0.1390**	0.4076	**0.3183**	**0.0916**	0.2768

dices CQ_{max} and CQ(1,1) have a similar performance while the SSIM index has the lowest association with the MOS. The highest values of correlation are associated with coefficients CQ(1,1) and CQ_{max} in both cases (Spearman and Kendall coefficients).

4.2. Evaluating Directional Distortions

A second numerical study explores the behavior of the CQ_{max} index when there is directional contamination in one of the images to be used. The directional contamination introduced in one of the images has been made using a variant of the contamination algorithm developed by Vallejos et al. (2015b). In this case the contamination is controlled by a parameter $\alpha \in \mathbb{R}$, which acts as a weight for the increment of the original image and can be interpreted as the intensity or level of directional contamination as is depicted in Algorithm 1. The directional contamination worsens the performance of most of the image quality measures. If the direction of contamination is known, the codispersion coefficient is able to recover the spatial association between the images (Vallejos et al., 2016).

In order to explore how Algorithm 1 works, and the effect of the parameter α, we contaminated images I23 and I04 from the TID2008 database. These images can be observed in Figure 4. The images look darker when α increases. In particular, the images look brighter for negative values of α. This behavior is independent of the direction of contamination. In addition, we compute the SSIM, CQ and CQ_{max} coefficients between image I23 and several contaminated images in the direction (1,1) with $\alpha \in \{-10, -7, -5, -1, 1, 5, 7, 10\}$. In Table 3 we report the three coefficients for the directions $(1,0), (1,1), (0,1), (1,1)$. The highest values of similarity are attained for the CQ_{max} coefficient which, in some cases, coincide with the CQ values for direction of contamination $(1,1)$. These values are uniformly larger than the values yielded by the SSIM index for all α. In Table 4 the same pattern is observed for image I04 where the contamination is in the direction $(0,2)$ and for

$$\alpha \in \{-1, -0.9, -0.8, -0.7, -0.6, -0.5, -0.4, -0.3, -0.2, -0.1\}.$$

CQ_{max} indicates maximum similarity between the original and transformed images. When α decreases to zero the behavior of CQ(1,1) gets worse, however, the behavior of SSIM and CQ_{max} are comparable enhancing the performance of CQ_{max} with respect

Algorithm 1: Transformation algorithm in the direction $\boldsymbol{h} = (1, 1)$ weighted by the parameter α.

input : An image $\boldsymbol{I}$ of size $n \times m$ and α
output: An image $\boldsymbol{Z}$ of size $n \times m$

```
for i = 1, 2, ..., n do
    for j = 1, 2, ..., m do
        if (i == 1) or (j == 1) then
            Z[i, j] ⟵ Simulation of a standard normal random variable;
        end
        else
            Z[i, j] ⟵ Z[i − 1, j − 1] + α · (I[i, j] − I[i − 1, j − 1])
        end
    end
end
Z ⟵ (Z − min Z) / (max Z − min Z);
return Z;
```

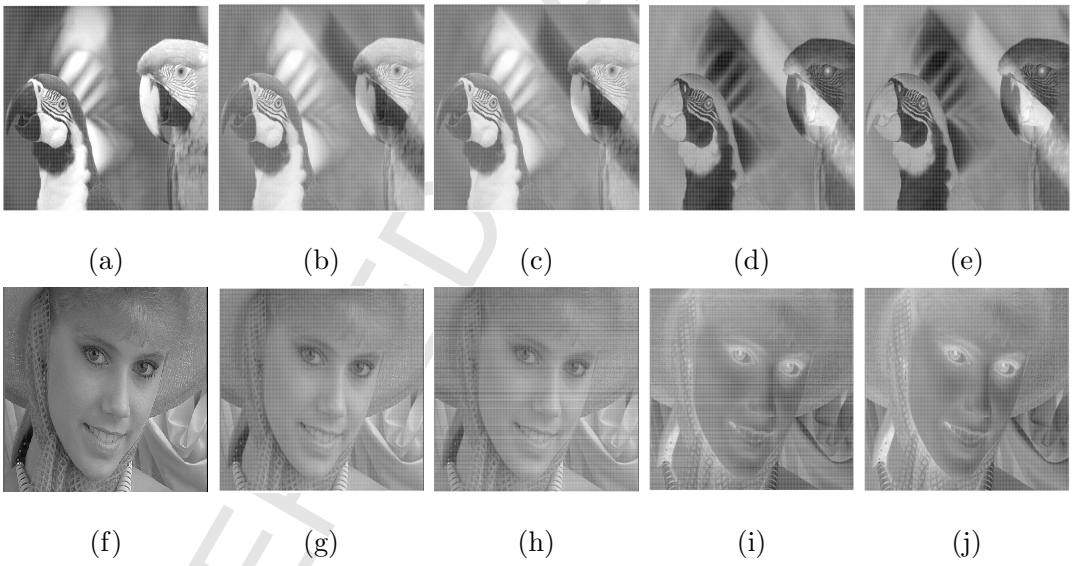

Figure 4: (a) Original image I23 from the TID2008 database. (b)–(e) directional contamination in the direction $(1, 1)$, for α =-5, -1, 1, and 5, respectively. (f) Original image I04 from the TID2008 database. (g)–(j) directional contamination in the direction $(0, 2)$, for α =-0.5, -0.1, 0.1, and 0.5, respectively.

to the SSIM index. Other experiments carried out with real images belonging to the TID2008 database (not shown here) confirm a similar behavior between SSIM and $\mathrm{CQ}_{\max}$.

Table 3: Similarity between band 1 of image I23 and its corresponding contaminations in the direction (1,1) for $\alpha \in \{-10, -7, -5, -1, 1, 5, 7, 10\}$.

	Image I23							
α :	-10	-7	-5	-1	1	5	7	10
SSIM	0.8421	0.8421	0.8422	0.8410	0.8266	0.8281	0.8277	0.8279
CQ(1,1)	0.9688	0.9688	0.9694	0.9672	0.9504	0.9526	0.9522	0.9524
CQ(1,-1)	0.9478	0.9477	0.9482	0.9420	0.9260	0.9316	0.9316	0.9317
CQ(1,0)	0.9495	0.9493	0.9502	0.9422	0.9245	0.9332	0.9334	0.9334
CQ(0,1)	0.9458	0.9456	0.9467	0.9374	0.9196	0.9295	0.9297	0.9298
CQ_{max}	**0.9692**	**0.9692**	**0.9694**	**0.9676**	**0.9508**	**0.9530**	**0.9526**	**0.9528**

Table 4: Similarity between band 1 of image I04 and its corresponding contaminations in the direction (0,2) for $\alpha \in \{-1, -0.9, -0.8, -0.7, -0.6, -0.5, -0.4, -0.3, -0.2, -0.1\}$.

	Image I04									
α :	-1	-0.9	-0.8	-0.7	-0.6	-0.5	-0.4	-0.3	-0.2	-0.1
SSIM	0.9894	0.9894	0.9891	0.9884	0.9882	0.9875	0.9857	0.9824	0.9725	0.9265
CQ(1,1)	0.8064	0.8087	0.8038	0.7963	0.7962	0.7964	0.7792	0.7513	0.7078	0.5176
CQ_{max}	**0.9988**	**0.9988**	**0.9989**	**0.9989**	**0.9987**	**0.9984**	**0.9983**	**0.9977**	**0.9961**	**0.9922**
α :	1	0.9	0.8	0.7	0.6	0.5	0.4	0.3	0.2	0.1
SSIM	0.9873	0.9873	0.9870	0.9862	0.9859	0.9853	0.9831	0.9804	0.9750	0.9365
CQ(1,1)	0.8031	0.8089	0.8038	0.8028	0.7972	0.7951	0.7777	0.7621	0.7236	-0.5573
CQ_{max}	**0.9968**	**0.9965**	**0.9966**	**0.9960**	**0.9962**	**0.9960**	**0.9956**	**0.9954**	**0.9969**	**0.9961**

5. An Application to Image Fusion

Image fusion (IF) in general is a methodology to extract information commonly acquired in several different domains. The main goal is to integrate the information contained in several images into one new image with a better quality that could not have been obtained otherwise (Flusser et al, 2007). This improved information can be used later for decision making (Hall and Llinas, 1997). In simple words it is the combination of two or more different images to form a new one by using a certain algorithm (Van Genderen and Pohl, 1994).

In the past decades, IF has been widely used in several applications and fields such as pattern recognition, visual enhancement, object detection and surveillance (Pohl and Van Genderen, 1998), among others. A recent review of remote sensing IF methods can be found in Ghassemian (2016). Different metrics about the quality of fused images is in Jagalingam and Hegbe (2015).

Here we show how the coefficient CQ_{max} helps to define a new IF algorithm when there are at least two available contaminated images as the input information and the original image is unknown. We assume that the first blurred image can be classified in one of the usual non-directional contaminations, e.g. additive Gaussian noise or JPEG2000 transmission errors. The second available image has been contaminated with a directional component, for instance using Algorithm 1. Better quality from

the available information could be of interest for example in outlier detection by using directional outlyingness measures in image processing and video, according to the guidelines given by Rousseeuw et al. (2016).

As an illustration we considered image I01 of the TID2008 database shown in Figure 5(a). This image has been contaminated with additive Gaussian noise (b) and JPEG2000 transmission errors (c). In addition, we used Algorithm 1 to yield a contaminated image in the direction $(1, 0)$ (d), and another contaminated image in the direction $(1, 1)$ (e). The goal is to obtain an estimation of image I01 from one contaminated image in the usual way ((b) or (c)) and another directionally contaminated in the direction (1,1) (e), with $\alpha = 5$.

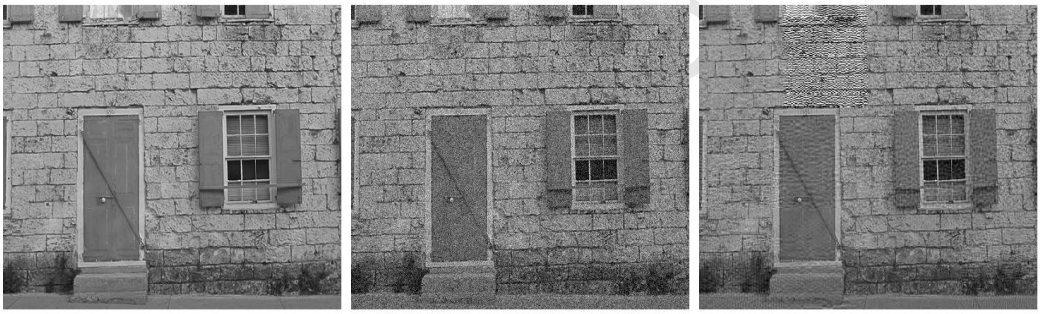

(a) (b) (c)

(d) (e)

Figure 5: (a) Original image I01; (b) - (c) Two distorted versions of image a) with different type and level of contamination; (d) - (e) Transformations of image a) in the horizontal and oblique (45°) directions.

Assume that $\boldsymbol{X}$ is an unknown $n \times m$ image to be reconstructed from the available images $\boldsymbol{Y}$ and $\boldsymbol{Z}$, where $\boldsymbol{Y}$ is a contaminated image in the usual way and $\boldsymbol{Z}$ is a contaminated version of $\boldsymbol{X}$ in the direction $\boldsymbol{h} = (h_1, h_2)$. In order to determine the valid values of h_1 and h_2, suppose that for all (i, j), $\max(1, 1+h_1) \leq i \leq \min(n, n+h_1)$ and $\max(1, 1 + h_2) \leq j \leq \min(m, m + h_2)$. **The directional contamination in**

image processing has not been studied under this perspective, in which it is assumed that $\boldsymbol{Z}$ follows the model

$$\boldsymbol{Z}_{i,j} = \boldsymbol{Z}_{i-h_1,j-h_2} + \alpha(\boldsymbol{X}_{i-h_1,j-h_2} - \boldsymbol{X}_{i,j}), \tag{16}$$

where $\boldsymbol{h}$ and α are unknown parameters, and $\boldsymbol{Z}_{1,l}$, $\boldsymbol{Z}_{k,1}$ are realizations of a standard normal random variable (boundary conditions) for all k and l. This proposal is based on empirical evidence showing that model (16) is a successful way to introduce directional noise on an image as is illustrated in Figures 4 and 5 (d),(e).

Then we can state the Algorithm 2.

Algorithm 2: Algorithm to reconstruct image $\boldsymbol{X}$ from images $\boldsymbol{Y}$ and $\boldsymbol{Z}$

---

input : Images $\boldsymbol{Y}$ and $\boldsymbol{Z}$ of size $n \times m$
Directions $\boldsymbol{h}^i = (h_1^i, h_2^i),\ i = 1, 2, \ldots, n$

output: $\widehat{\boldsymbol{X}}$, an estimation of $\boldsymbol{X}$

1 Compute $\mathrm{CQ}_{\max}$ between $\boldsymbol{Y}$ and $\boldsymbol{Z}$ according to (12) and keep the direction of maximum codispersion, called $\widehat{\boldsymbol{h}} = (\widehat{h}_1, \widehat{h}_2)$

2 Estimate α as

$$\widehat{\alpha} = \mathrm{median}(A),$$

where

$$A = \left\{ \frac{\boldsymbol{Z}_{i,j} - \boldsymbol{Z}_{i-\widehat{h_1},j-\widehat{h_2}}}{\boldsymbol{Y}_{i-\widehat{h_1},j-\widehat{h_2}} - \boldsymbol{Y}_{i,j}} : (i,j), (i-\widehat{h_1}, j-\widehat{h_2}) \in W, (\boldsymbol{Y}_{i-\widehat{h_1},j-\widehat{h_2}} - \boldsymbol{Y}_{i,j}) \neq 0 \right\}$$

and W is as in (1);

3 Estimate $\boldsymbol{X}$ as

$$\widehat{\boldsymbol{X}}_{i,j} = \boldsymbol{Y}_{i-\widehat{h}_1,j-\widehat{h}_2} - \frac{\boldsymbol{Z}_{i,j} - \boldsymbol{Z}_{i-\widehat{h}_1,j-\widehat{h}_2}}{\widehat{\alpha}}$$

4 **return** $\widehat{\boldsymbol{X}}$;

From Equation (16) we have that

$$\alpha = \frac{\boldsymbol{Z}_{i,j} - \boldsymbol{Z}_{i-h_1,j-h_2}}{\boldsymbol{X}_{i-h_1,j-h_2} - \boldsymbol{X}_{i,j}}. \tag{17}$$

Because $\boldsymbol{X}$ is unknown, the equation described in step 2 of Algorithm 2 is obtained by **replacing $\boldsymbol{X}$** by $\boldsymbol{Y}$ in Equation (17) and by using the estimation of $\boldsymbol{h}$ obtained in step 1.

In step 2, the median filter was considered due to its robustness (Kashyap and Eom, 1988; Qiu, 1996).

One of the reasons why Algorithm 2 is able to recover $\boldsymbol{X}$ from $\boldsymbol{Z}$ and $\boldsymbol{Y}$, is that from Equation (16) the increments of $\boldsymbol{Z}$ in the direction $\boldsymbol{h}$ are a linear combination of the increments of $\boldsymbol{X}$ in the same direction. Estimating $\boldsymbol{h}$

and the increments of $\boldsymbol{X}$ from the increments of $\boldsymbol{Y}$, it is possible to provide an estimation of α and subsequently an estimation $\widehat{\boldsymbol{X}}$ of $\boldsymbol{X}$.

We explored the performance of Algorithm 2 considering the first band of all images belonging to the TID2008 database. The image $\boldsymbol{Y}$ corresponds to the 1700 distorted images of the database (25 different images affected by 17 types of contamination with 4 levels of intensity). The image $\boldsymbol{Z}$ was generated for the 25 original images using the algorithm developed in Vallejos et al. (2015b). The original images were divided into four groups. The first group of seven images was contaminated in the direction $(1, 0)$. The second group containing 6 images was contaminated in the direction $(0, 1)$. The third group of 6 images was contaminated in the direction $(1, 1)$, and the last group of 6 images was contaminated in the direction $(1, -1)$. Considering these groups we explored the percentage of restored images as a function of the spatial lag in which the original images were directionally contaminated. Table 5 describes the images

Table 5: Percentage of restored images as a function of the spatial lag in which the original image was directionally contaminated.

	$(1,0)_{N=476}$	$(0,1)_{N=408}$	$(1,1)_{N=408}$	$(1,-1)_{N=408}$
Images	01,02,04,06, 09,17,25	03,08,10 11,12,19	05,13,14 16,18,21	07,15,20 22,23,24
Yes	291 (61%)	299 (73%)	407 (99.9%)	399 (98%)
No	185 (39%)	109 (27%)	1 (1%)	9 (2%)

belonging to each of the four groups, the directions of interest, and the percentage of correct restoration. An image is considered correctly restored if Algorithm 2 (step 1) is able to detect the true direction of contamination. The highest percentage of correct restoration is associated with the spatial lags $(1, 1)$ and $(1, -1)$. At least 61% of the images that were contaminated in the horizontal or vertical directions were correctly restored. In addition, another experiment was carried out to explore the performance of the restauration algorithm as a function of the 17 types of noise for image $\boldsymbol{Y}$. For each type of contamination, 100 simulation runs were considered (25 images with 4 different levels of contamination). Table 6 shows that the lowest percentage of restoration (59%) is associated with contaminations 04 (masked noise) and 05 (high frequency noise), while the highest percentage of restoration (99%) is achieved for contaminations 16 (mean shift) and 17 (contrast change).

As an example, we considered image I01 from the TID2008 database. This image was directionally contaminated using $\boldsymbol{h} = (1, 0)$ with $\alpha = 1$. The non-directionally distorted image $\boldsymbol{Y}$ was considered having quantization noise with intensity level 4. Then using Algorithm 2 the restored image was generated. The results can be seen in Figure 6(d). We also report the similarity coefficients between each pair of images shown in Figure 6 (see Table 7). The similarity coefficients SSIM, CQ, and CQ_{max} are able to capture the similarity between the original and restored images (a) and

Table 6: Percentage of restored images for the 17 types of contamination present in the TID2008 database.

	Type of Contamination								
	01	02	03	04	05	06	07	08	09
%	70%	72%	96%	59%	59%	71%	85%	85%	82%
	10	11	12	13	14	15	16	17	
%	83%	80%	86%	83%	93%	94%	99%	99%	

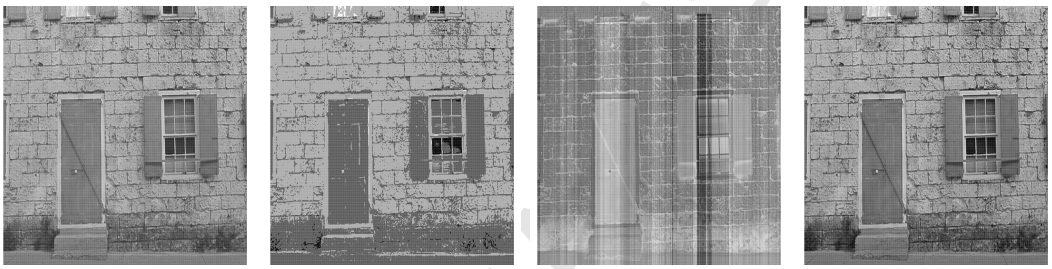

(a) (b) (c) (d)

Figure 6: (a) Original image I01; (b) Image (a) distorted by using quantization noise with level of intensity equal to 4; (c) Directional contamination of image (a) in the direction $(1, 1)$ with $\alpha = 1$; (d) Restored image by Algorithm 2.

(d). However, the CQ_{max} is able to capture the correlation between the original and the horizontally contaminated images (a) and (c), while the other coefficients provide reverse sign correlation. This highlights the goodness of CQ_{max} to afford suitable directional information.

Table 7: Coefficient SSIM, CQ(1,1), and CQ_{max} for the images of Figure 6.

	Similarity			
Index	(a) and (b)	(a) and (c)	(a) and (d)	(b) and (d)
SSIM	0.8362	-0.6593	0.9551	0.8510
CQ(1,1)	0.6974	-0.7901	0.9547	0.7095
CQ_{max}	0.7027	0.9928	0.9548	0.7149

6. Conclusions and Final Remarks

We have introduced the CQ_{max} index which computes the maximum codispersion among a fixed number of directions on the plane. Such a coefficient defines a pseudo-metric that, according to the empirical evidence provided in this paper, preserves the information. In addition, the computation of the CQ_{max} index brings the direction associated with the maximum codispersion which was used as a middle step to create a restoration algorithm from two distorted images, one with any conventional noise and the other with directional error. The empirical experiments highlight the performance of CQ_{max} over previous indices SSIM and CQ.

Algorithm 2 needs further exploration to gain insight into the advantages and limitations. First, the number of different directional contaminations in an image is a crucial point in the estimation process. In Figure 7 we display an image that has been contaminated three times sequentially with directional noise. In general, the SSIM, CQ and CQ_{max} indices do not have a satisfactory performance when dealing with more than one directional noise (Vallejos et al., 2016). Alternative coefficients used to account for similarity under small rotations (Sampat et al., 2009) could perform better in this respect. Second, in all developed experiments, the direction of contamination coincides with one of the 32 directions considered in the implementation algorithm depicted in Algorithm 3. Further experiments are needed to explore the performance of Algorithm 2 when the direction of contamination is arbitrary. Third, the restoration yielded by the algorithm strongly depends on the estimation of α. In our experience, when $\alpha \in (0, 1)$ the restoration is worst than the case when $|\alpha| > 1$. Based on the

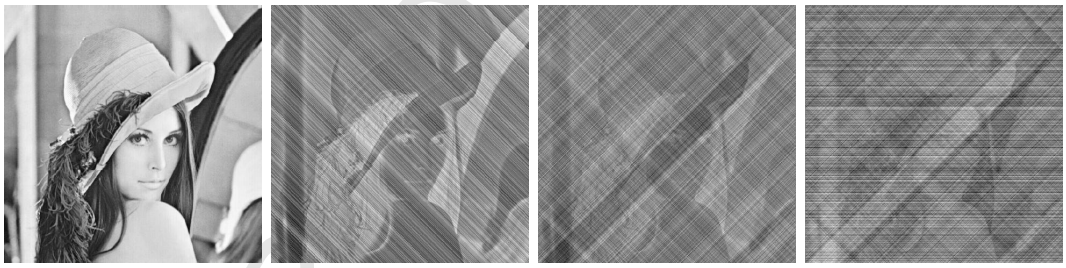

(a) (b) (c) (d)

Figure 7: (a) Original image; (b) Image (a) contaminated in the direction (1,1) with $\alpha = 5$; (c) Image (b) contaminated in the direction (1,-1) with $\alpha = -1$; (d) Image (c) contaminated in the direction (0,1) with $\alpha = 1$

pseudo distance metric associated with the CQ_{max} index, a modified measure could be constructed for which the quasi-convexity, a region of convexity around the minimizer, and distance preservation under orthogonal and unitary transformations are of great interest (Brunet et al., 2012). We leave the considered problems as topics of our future studies.

7. Acknowledgements

Silvia Ojeda and Grisel Britos were supported by Secyt-UNC grant (Res. Secyt 313/2016.) and CIEM-CONICET, Argentina. Ronny Vallejos was partially supported by AC3E, FB–0008, Chile. The authors want to express their sincere gratitude to Aaron Ellison, Felipe Osorio, Francisco Cuevas, and Jonathan Acosta for helpful discussions and support.

Appendix

A. Algorithm to Compute $\mathbf{CQ_{max}}$

Algorithm 3: $\mathrm{CQ}_{\max}$ index for 32 directions (h_1, h_2)

input : Images $\mathbf{X}$ and $\mathbf{Y}$ of size $N \times M$ and $\mathrm{CQ}(h_1, h_2)$
output: $\mathrm{CQ}_{\max}$

Let v_1 and v_2 vectors of size 15×1 and 17×1 respectively.
$i = 0$; $j = 0$
for $h_1 = 1, ..., 5$ **do**
  for $h_2 = 0, ..., (h_1 - 5)$ **do**
    $i \leftarrow i + 1$
    $v_1[i] \leftarrow \mathrm{CQ}(X, Y, h_1, h_2)$
  end
end
for $h_1 = 0, ..., 2$ **do**
  for $h_2 = 1, ..., 4$ **do**
    $j \leftarrow j + 1$ $v_2[j] \leftarrow \mathrm{CQ}(X, Y, h_1, h_2)$
  end
end
$v_2[13] \leftarrow \mathrm{CQ}(X, Y, 3, 1)$
$v_2[14] \leftarrow \mathrm{CQ}(X, Y, 3, 2)$
$v_2[15] \leftarrow \mathrm{CQ}(X, Y, 4, 1)$
$v_2[16] \leftarrow \mathrm{CQ}(X, Y, 4, 2)$
$v_2[17] \leftarrow \mathrm{CQ}(X, Y, 0, 5)$
$\mathrm{CQ}_{max} \leftarrow \max(|(v_1, v_2)|)$
return CQ_{max};

References

Base, G. C., Reinsel, S. 1993. Properties of the spatial unilateral first-order ARMA model. Advances in Applied Probability 25, 631–648.

Brunet, D., Vrscay, E.R.,Wanng, Z., 2012. On the mathematical properties of the structural similarity index. IEEE Trans. Image Process 21, 1488–1498.

Buckley, H. L., Case, B.S., Ellison, A. M., 2016a. Using codispersion analysis to characterize spatial patterns in species co-occurrences. Ecology 97, 32–39.

Buckley, H. L., Case, B. S., Zimmermann, J., Thompson, J., Myers, J.A., Ellison, A. M., 2016b. Using codispersion analysis to quantify and understand spatial patterns in species-environment relationships. New Phytologist 211, 735–749.

Chandler, D. M., Hemami, S. S., 2007. VSNR: A wevelet-based visual sinal-to-noise-ratio for natural images. IEEE Trans. Image Process 9, 2284-2298.

Cheung, F. J. F., Heskiaoff, H., Billis, S. H., Cheng, P. S. 2000. Directional line detectors in correlated noisy environments. IEEE Transactions on Image Processing 9, 2061–2070.

Clifford, P., Richardson, S., Hémon, D., 1989. Assessing the significance of the correlation between two spatial processes. Biometrics 45, 123–134.

Crosby, D. S., Breaker, L. C., Gemmill, W. H., 1993. A proposed definition for vector correlation in Geophysics: Theory and application. Jounal of Atmospheric and Oceanic Technology 10, 355–367.

Cuevas, F., Porcu, E., Vallejos, R., 2013. Study of spatial relationships between two sets of variables: A nonparametric approach. Journal of Nonparametric Statistics 25, 695-714.

Dutilleul P., 1993. Modifying the t test for assessing the correlation between two spatial processes. Biometrics 49, 305–314.

Duttilleul, P., Pelletier, B., Alpargu, G., 2008. Modified F tests for assessing the multiple correlation between one spatial process and several others. Journal of Statistical Planning and Inference 138,1402–1415.

Eckert, M. P., Bradley, A. P., 1998. Perceptual quality metrics applied to still image compression. Signal Processing 70, 177–200.

Flusser, J., Šroubek, F., Zitová, V., 2007. Image Fusion: Principles, Methods, and Applications. Tutorial EUSIPCO. Institute of Information Theory and Automation, Academy of Sciences of the Czech Republic.

Ghassemian, H., 2016. A review of remote sensing image fusion methods. Information Fusion 32, 75-89.

Hall, L., Llinas, J., 1997. An introduction to multisensor data fusion. Proceedings of the IEEE 85, 6-23.

Hollander, M., Wolfe, D. A., Chicken, E., 2014. Nonparametric Statistical Methods. Wiley, New Jersey.

Isaaks, E. H. and Srivastava, R. M., 1989. An Introduction to Applied Geostatistics, Oxford University Press, New York.

Jagalingam, P., Hegbe, A. V., 2015. A review of quality metrics for fused image. Aquatic Procedia 4, 133–142.

Jupp, P. E., Mardia, K. V., 1980. A general correlation coefficient for directional data and related regression problems. Biometrika 67, 163–173.

Kashyap, R., Eom, K., 1988. Robust images techniques with an image restoration application. IEEE Trans. Acoust. Speech Signal Process 36, 1313–1325.

Larson, E. C., Chandler, D. M., 2010. Most apparent distortion: Full-reference image quality assessment and the role of strategy. Journal of Electronic Imaging 19, 011006.

Ma, K., Zeng, K., Wang, Z., 2015. Perceptual quality assessment for multi-exposure image fusion. IEEE Transactions on Image Processing 24, 3345–3356.

Matheron, G., 1965. Les Variables Régionalisées et leur Estimation. Masson, Paris.

Ojeda S. M., Vallejos R. O., Lamberti P. W., 2012. Measure of similarity between images based on the codispersion coefficient. Journal of Electronic Imaging 21, 023019.

Osorio F, Vallejos R., Cuevas, F., 2012. `SpatialPack` - An R package for computing the association between two spatial or temporal processes. R package version 0.2-3, URL:http://cran.r-project.org/package=SpatialPack

Pistonesi, S., Martinez, J., Ojeda, S., Vallejos, R., 2015. A novel quality image fusion assessment based on maximum codispersion. Lecture Notes in Computer Science 9423, 383–390.

Pohl, C., Van Genderen, J. L., 1998. Multisensor image fusion in remote sensing: concepts, methods and applications. Int. J. Remote Sens19, 823–854.

Ponomarenko, N., Lukin, V., Zelensky, A., Egiazarian, K., Carli, M., Battisti. M., 2009. Tid2008-a database for evaluation of full-reference visual quality assessment metrics. Advances of Modern Radioelectronics 10, 30–45.

Ponomarenko N., Ieremeiev O., Lukin V., Egiazarian K., Jin L., Astola J., Vozel B., Chehdi K., Carli M., Battisti F., and Jay Kuo C., 2013. Color image database TID2013: Peculiarities and preliminary results, 4th European Workshop on Visual Information Processing EUVIP2013, pp.106-111.

Qiu, G., 1996. An improved recursive median filtering scheme for image processing. IEEE Transactions on Image Processing 5, 646-648.

Rousseeuw, P., Raymaekers, J., Hubert, M., 2016. A Measure of Directional Outlyingness with Applications to Image Data and Video. arXiv:1608.05012

Rukhin A., Vallejos, R., 2008. Codispersion coefficient for spatial and temporal series. Statistics & Probability Letters 78, 1290–1300.

Sampat, M. P., Wang, Z., Gupta, S., Bovik, A. C., 2009. Complex wavelet structural similarity: a new image similarity index. IEEE Trans. Image Process. 18, 2385–2401.

Sheikh, H. R., Bovik C., 2006. Image information and visual quality. IEEE Trans. image Process. 15, 430–444.

Vallejos, R., 2008. Assessing the association between two spatial or temporal sequences. Journal of Applied Statistics 35, 1323–1343.

Vallejos, R., 2012. Testing for the absence of correlation between two spatial or temporal sequences. Pattern Recognition Letters 33, 1741–1748.

Vallejos, R., Mallea, A., Herrera, M., Ojeda, S., 2015a. A multivariate geostatistical approach for landscape classification from remotely sensed image data. Stochastic Environmental Research and Risk Assessment 29, 369–365.

Vallejos, R., Osorio, F., Mancilla, D., 2015b. The codispersion map: a graphical tool to visualize the association between two spatial processes. Statistica Neerlandica 69, 298–314.

Vallejos, R., Mancilla, D., Acosta, J., 2016. Image similarity assessment based on coefficients of spatial association. Journal of Mathematical Imaging and Vision 56, 77–98.

Van Genderen, J. L., Pohl, C., 1994. Image fussion: Issues, techniques and applications. Intellingent Image Fusion, Proceedings EARSeL Workshop, Strasbourg, France, 11 September 1994, edited by J. J. Van Genderen and J. Cappellini, pp. 18-26.

Wang Z., Bovik A., 2002. A universal image quality index. IEEE Signal Processing Letters 9, 81–84.

Wang, Z., Zimoncelli E.P., Bovik, C., 2003. Multi-scale structural similarity for image quality assesment. in Proc. IEEE Asilomar Conf. Signals Syst. Comput., Pacific Grove, CA:1398–1402.

Wang, Z., Bovik, A., Sheikh, H. R., Simoncelli, E. P., 2004. Image quality assessment: from error visibility to structural similarity. IEEE Transactions on Image Processing 13, 1–14.

Wang Z., Bovik A., 2009. Mean squared error: love it or leave it? a new look at signal fidelity measures. IEEE Signal Process Magazine 26, 89–117.

Wang, Z., Li, Q., 2011. Information content weighting for percentual image quality assessment. IEEE Trans. Image Process. 20, 1185–1198.

Wang, S. Rehman, A. Wang, Z., Ma, S., Gao, W., 2012. SSIM-motivated rate-distortion optimization for video coding. IEEE Transactions on Circuits and Systems for Video Technology 22, 516–529.

Zhang, L., Zhang, L., Mou, X., Zhang, D., 2011. A feature similarity index for image quality assessment. IEEE Trans. Image Process. 20, 2378–2386.